Journal of Applied Polymer Science

Biopolyester-based nanocomposites: Structural, thermo-mechanical and biocompatibility characteristics of poly(3-hydroxybutyrate)/ montmorillonite clay nanohybrids

Elpiniki Panayotidou,[1,2] Anthoula Kroustalli,[3] Apostolos Baklavaridis,[1] Ioannis Zuburtikudis,[1*] Dimitris S. Achilias,[2] Despoina Deligianni[3]

[1]The Nanomaterials and Manufacturing Processes Laboratory (NanoMaMa Lab), Department of Mechanical and Industrial Design Engineering, TEI of Western Macedonia, 50100 Kozani, Greece

[2]Laboratory of Organic Chemical Technology, Department of Chemistry, Aristotle University of Thessaloniki, 54124 Thessaloniki, Greece

[3]Laboratory of Biomechanics and Biomedical Engineering, Department of Mechanical Engineering and Aeronautics, University of Patras, 26504 Rio, Greece

*Present address: Department of Chemical and Petroleum Engineering, United Arab EmiratesUniversity, Al Ain, UAE

Correspondence to: I. Zuburtikudis (E-mail: izub@teikoz.gr or ioannis.z@uaeu.ac.ae)

ABSTRACT: In this work, the structural, thermal, mechanical, and biocompatibility characteristics of biopolyester-based nanocomposites with phyllosilicate clays, namely those of poly(3-hydroxybutyrate) (PHB) with octadecylamine-modified montmorillonite (C_{18}MMT), are reported. PHB/clay nanocomposites with various loadings were prepared by melt mixing. X-ray diffraction measurements and transmission electron microscopy images revealed the coexistence of intercalated and exfoliated states in the produced nanocomposites. Atomic force microscopy imaging also shed light to the morphological characteristics of the pure PHB and the prepared nanocomposites. The thermal stability of the nanohybrid materials was improved with the 5 wt % loading nanocomposite to show the best improvement. In addition, the nanohybrids have lower melting point compared to pure PHB and enhanced storage modulus (E'). Finally, the biocompatibility of pristine PHB and the 5 wt % nanocomposite was assessed by studying the morphology and proliferation of osteoblast cells attached on their surfaces. The results after 3 and 7 days of cell culturing indicate the incorporation of nanoclays does not change the cell adhesion and spreading as compared to those on pure PHB. © 2014 Wiley Periodicals, Inc. J. Appl. Polym. Sci. **2015**, *132*, 41628.

KEYWORDS: biocompatibility; clay; composites; extrusion; properties and characterization

Received 14 July 2014; accepted 12 October 2014
DOI: 10.1002/app.41628

INTRODUCTION

Biodegradable polymers are environmentally benign and have attracted the interest of many researchers recently.[1–4] An interesting and very attractive group of biodegradable polymers is the polyhydroxyalkanoates (PHAs), which constitute a class of microbial biopolyesters that are produced from renewable resources.[5–7] The most prominent and widely studied member of PHAs is polyhydroxybutyrate (PHB). Maurice Lemoigne, a French microbiologist, identified and characterized it in 1925. It can be produced by microorganisms such as *Alcaligeneseutrophus*, *Bacillus Megaterium* and is used as an intracellular storage for energy and carbon.[7–11] PHB is an isotactic polymer with an R configuration. It has a lower hydrolytic degradation rate compared to the other biodegradable polymers and mechanical properties comparable to those of polypropylene (PP). As a result, it can be a potential substitute of PP, which is an oil-derived polymer. However, the biocompatibility and ability of PHB to bio-degrade in every environment are considered as the most interesting properties.[11–13] Recently, a lot of studies (both *in vivo* and *in vitro*) have researched the compatibility of PHB to various cell lines such as osteoblast, epithelium, blood, and bone tissue and concluded that PHB is fully compatible to these cells.[14,15] Therefore, PHB is a promising candidate material in biomedical applications and especially, in tissue engineering. It can be used in drug delivery systems, in heart valves,

Logo of funding program, Heracleitos II.

cardiovascular devices, pericardial patches, sutures, skin substitutes, nerve cuffs, surgical meshes, and others.[16–18] PHB is also a piezoelectric material, which facilitates osteogenesis induction.[19] However, the fragility, brittleness and the fact that it degrades near its melting point make the processing of PHB difficult and restrict the field of application. Some of the solutions proposed to surpass these disadvantages are: (a) biosynthesis of copolymers of PHB with other hydroxyalkanoate monomers, (b) preparation of blends incorporating PHB and another biopolymer, and (c) synthesis of PHB based block copolymers. The fabrication of PHB nanocomposites consists an alternative proposal and is investigated in this work.[20–25]

Mixtures consisting of a polymeric matrix and fillers with at least one dimension in nanoscale are characterized as polymer nanocomposites. It has been proved that at low concentrations of nanofiller, usually up to 5 wt %, the mechanical properties and the thermal behavior of these hybrid materials are improved.[24] Clay minerals, which are eco-friendly and cheap, are the most commonly used nanofillers commercially. The most important among these clay nanofillers is montmorillonite. For the fabrication of polymer nanocomposites with enhanced properties the modification of montmorillonite is required, so that it becomes compatible with the polymer matrix. Montmorillonite is frequently organo-modified by a reaction in which the alkyl ammonium cations substitute the sodium ones.[26]

PHB was first suggested for medical applications in 1962 for biodegradable surgical sutures and tissue healing films. But the real revolution in PHB's uses in biomedical applications was held since 1980.[27]

All these years, copolymers of PHB with other hydroxyalkanoates, such as 3-hydroxyvalerate, 3-hydroxyhexanoate, 3-hydroxyoctanoate, were found to be appropriate for tissue engineering applications.[28]

A number of *in vivo* studies have shown no inflammatory reaction after PHB implantation, for example as nonwoven patches as pericardial substitutes in sheep.[27]

In bone tissue engineering applications, PHB is a particularly interesting biopolymer for several different reasons. First, the bone tissue adaptation response was consistently positive for a period of up to 12 months. Second, no expanded structural breakdown was observed *in vivo*.[29] PHB/Hydroxyapatite composites have been found to provoke fast bone healing and formation of new bone substance.[27] In another study, composites of PHB with 10 and 20 wt % loading of hydroxyapatite exhibited the greater differentiation and growth.[30] Composites of PHBV/wollastonite have shown improved differentiation and proliferation compared to the pure PHBV.[31] Similar results were observed in PHB nanocomposites with bioactive glass.[32]

The biocompatibility of nanocomposites of PHB with bioactive glass and hydroxyhapatite has been investigated extensively. However, biocompatibility studies of PHB nanocomposites with organomodified montmorillonite are limited.

In this work, nanohybrid materials of PHB with various loadings of organically modified montmorillonite with octadecylamine (C_{18}MMT) were produced by the melt-mixing technique. The objective was the production of novel hybrid materials with improved thermal and mechanical properties and to check their biocompatibility, since any biomedical application requires such a check. The combination of results presented here is the novelty of the current work. The authors hope that this work is valuable for the researchers, who focus on PHB hybrid materials for biomedical applications.

EXPERIMENTAL

Materials

Sigma Aldrich Chemical provided the neat polymer (PHB), which was used as received. Natural sodium montmorillonite (NaMMT) with a Cation Exchange Capacity (CEC)equal to 92.6 meq/100 g was purchased from Southern Clay Products (TX). All other chemicals, octadecylamine ($C_{18}H_{37}NH_2$), HCl (37% w/v), and ethanol absolute, were purchased by Sigma Aldrich Chemical Co.

Modification of Montmorillonite

Sodium montmorillonite was dried for 24 h at 80°C before use. Its modification took place via a cation exchange reaction between the natural montmorillonite and octadecylammonium salt, according to the procedure described in a previous study of ours.[33] The final product (organo modified montmorillonite or else OMMT or C_{18}MMT) was stored in a desiccator.

Nanocomposite Materials Preparation

The hybrid materials were produced by the melt mixing technique in a co-rotating twin-screw microextruder/compounder (HaakeMiniLab^{TM}). The isothermal drum temperature was kept at 175°C. Thermal degradation of the polymer was prevented by nitrogen flow inside the barrel. The mixture was mixed for 3 min at a screw speed of 130 rpm. Hybrids with loadings of 1, 3, 5, and 10 wt % were prepared.

Culture of Human Bone Marrow Cells

The cell aspiration was realized according to a well-established protocol.[34] The cell culture procedure that was followed is similar to that described in the work of Kokkinos *et al.*[35] Cells of first to third passage were cultured on five different culture substrates (pure PHB, 1, 3, 5, and 10 wt % PHB/clay nanocomposite) at a population density of 10,000 cells/cm^2.

Preparation of PHBs for Cell Culture

The samples were sterilized by autoclave (126°C) and, subsequently, they were dried and were exposed to ultraviolet light for 2 h.

Characterization Techniques

X-ray Diffraction. The structure of the organo-modified montmorillonite and that of the hybrid materials were investigated by X-ray diffraction (XRD). The measurements were carried out using Ni-filtered Cu K alpha radiation ($\lambda = 0.154$ nm) in 3003 TT Rich. Seifert diffractometer. The 2θ scanning range was varied from 1° to 10°, for the organo-modified montmorillonite and the hybrid materials and the measuring time per step (0.01°) was 15 s.

Transmission Electron Microscopy. An ultramicrotome (LEICA UC7) was employed for the preparation of the transmission

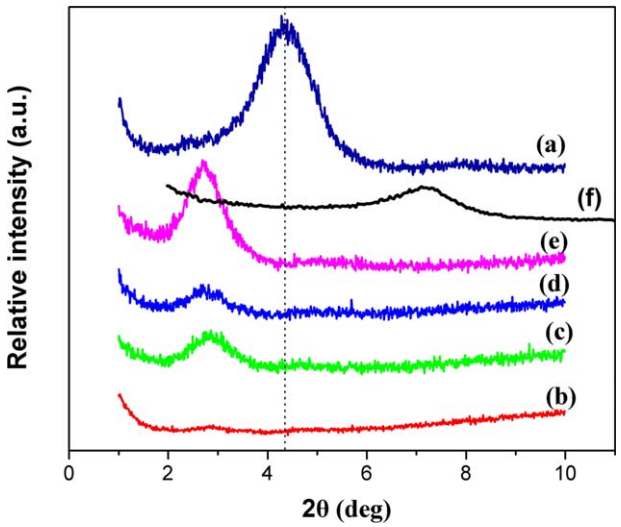

Figure 1. XRD diffraction patterns of pure C_{18}MMT (a) and PHB/ C_{18}MMT nanocomposites: 1 wt % (b); 3 wt % (c); 5 wt % (d); 10 wt % (e); and sodium montmorillonite (f). [Color figure can be viewed in the online issue, which is available at wileyonlinelibrary.com.]

electron microscopy (TEM) samples. Thin segments with thickness around 50 nm were cut at room temperature. These segments were placed on copper grids and were taken for observation in the TEM (JEM 1010) at 100 kV.

Atomic Force Microscopy. The nanohybrid surface was examined using Scanning Probe Microscopy (Veeco^{TM} CP-II) in atomic force microscopy (AFM) intermittent-contact mode. All images were recorded and analyzed via the instrument's software. Prior to the AFM observations, the PHB/clay nanocomposite sample surfaces were chemically etched with chloroform to reveal clean nanostructured surfaces.

Thermogravimetric Analysis. The effect of the nanofiller on the thermal stability of PHB was studied by thermogravimetric analysis (TGA). The measurements were done using Pyris 1 TGA Perkin-Elmer thermal analyzer. The experiments took place in nitrogen atmosphere at heating rate10°C/min.

Differential Scanning Calorimetry. Differential scanning calorimetry (DSC) was used for the evaluation of the melting point both for pure PHB and for the nanocomposite materials. A Diamond Perkin Elmer DSC devise was used for the DSC measurements. The samples were heated up to 190°C at 10°C/min and were kept at this temperature for 1 min. A cooling step was introduced subsequently and then the samples were heated up again to 190°C at 10°C/min.

Dynamic Mechanical Thermal Analysis. The viscoelastic properties for the nanohybrid materials and the neat polymer were examined by dynamic mechanical thermal analysis (DMTA). A Polymer Laboratories (Model PL-MKII) analyzer conducting bending head was used to record DMTA spectra. Measurements were performed at 1 Hz and the temperature was varied from −20 to 120°C with a step of 2°C/min. Rectangular films with length × width × thickness = 30 × 10 × 1 mm were prepared by thermo-pressing for the DMTA measurements.

Table I. $d_{(001)}$-Spacing of Natural Clay (NaMMT), Pure Organomodified Clay (C_{18}MMT), and C_{18}MMT Dispersed in the PHB Matrix

Samples	2θ (°)	$d_{(001)}$ (nm)
Sodium montmorillonite	7.22	1.2
Pure C_{18}MMT	4.37	2
PHB/1 wt % C_{18}MMT	No peak	-
PHB/3 wt % C_{18}MMT	2.83	3.12
PHB/5 wt % C_{18}MMT	2.72	3.24
PHB/10 wt % C_{18}MMT	2.69	3.28

Cell Morphology and Proliferation. Cell adhesion and morphology of osteoblast cells onto PHB and PHB/clay nanocomposite surfaces were examined by scanning electron microscopy (SEM). Cell-seeded PHB surfaces were incubated for 3 days. Phosphate-buffered saline was used to remove the unattached cells according to a well-established protocol.[34] All samples were coated with gold prior to SEM observations via a cold field emission SEM (JEOL-JSM 6300).

For the assessment of proliferation a well-established procedure was used.[31] Initially, cell-seeded substrates were stained by 4′,6-diamidino-2-phenylindole (DAPI). Subsequently, they were incubated for 3 and 7 days.

RESULTSAND DISCUSSION

Structure and Morphology Studies

X-ray Diffraction. The XRD study of the hybrid materials, the natural and the organo-modified montmorillonite was held in the range of $2\theta = 1°–10°$, according to the literature.[22,24] The results are presented in Figure 1. Bragg's law [eq. (1)] gives the relationship between the angle of the diffracted beam and the interplanar distance (d).

$$2d = n\lambda/\sin\theta \quad (1)$$

where n the reflection order ($n = 1$ for this work) and λ = the wavelength of the X-ray beam used (Cu-K alpha here). The results of applying Bragg's law are shown in Table I.

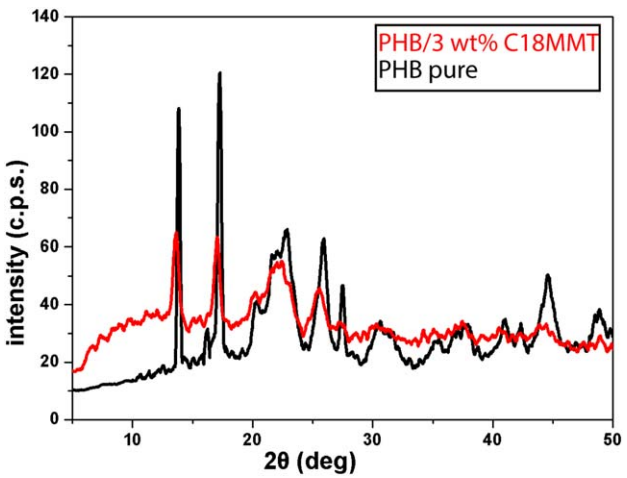

Figure 2. XRD diffraction patterns of pure PHB and the PHB/ 3 wt % C_{18}MMT hybrid material. [Color figure can be viewed in the online issue, which is available at wileyonlinelibrary.com.]

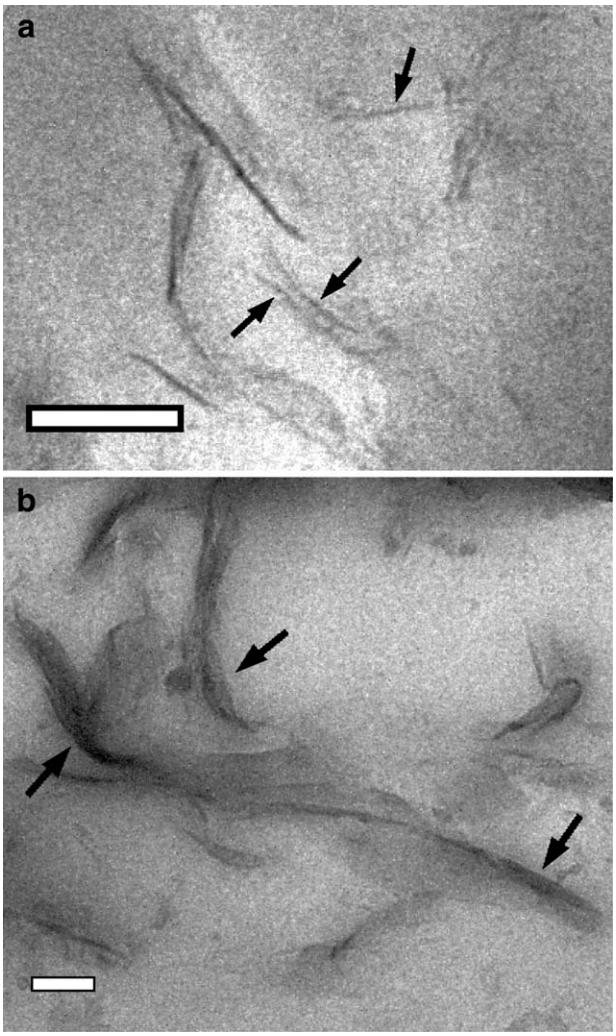

Figure 3. TEM images of PHB with 1 wt % C_{18}MMT (a) and 5 wt % C_{18}MMT (b). The bar is set to 100 nm.

By mixing the polymer with the organically modified clay, the polymer chains diffuse into the clay galleries and expand the distance between the clay platelets, as it is shown in Figure 1. This expansion is represented in the XRD patterns of Figure 1 by the shift of the characteristic peak to lower 2θ values. This shift means that the spacing between the layers becomes bigger in the hybrid materials than that of the organo-modified montmorillonite. As it is shown in Figure 1, a characteristic peak appears at $2\theta = 4.37^{\circ}$ proving that the basal d-spacing of the OMMT clay is 2 nm. Increasing the loading of the clay, an increment to the d-spacing of the hybrid materials is observed, as Table I shows: from 3.12 nm for the 3 wt % loading to 3.28 nm for the 10 wt % loading. All these experimental findings indicate that nanocomposite materials with intercalated structure were produced.[24] For the PHB/1 wt % C_{18}MMT nanocomposite, no distinct peak was observed. The peak absence may be attributed either to the exfoliated structure created or the insufficient amount of intercalated clay sheets leading to insufficient counts per second (cps) for the formation of an evident peak in the XRD spectra. Therefore, the XRD result for the1 wt % loading nanocomposite offers only an inconclusive suggestion that the 1 wt % nanohybrid is either in the exfoliated or the intercalated/exfoliated state.[22] This suggestion has to be confirmed by TEM and that is why TEM images are presented after the XRD results.

The crystalline structure of PHB was studied by many researchers. PHB crystallizes into two polymorphs, the α- and β-form. The α-form crystals are formed under the most common conditions: solution, cold, and melt crystallization. The β-form derives upon stretching.[36–49]

Based on the literature,[22] the addition of clay platelets does not affect the crystalline structure of PHB. Moreover, we also carried out XRD measurements for the pure PHB and the PHB/3 wt % C_{18}MMT hybrid material (presented in Figure 2). As it is shown in Figure 2, the presence of the organo-modified clay does not influence (there is no shift in) the characteristic peaks of the pure polymer. This is an indication that the crystalline form of PHB is unaffected by the addition of the clay.

Transmission Electron Microscopy. TEM was used in order to clarify the dispersion of the clay sheets in the nanocomposite materials. Images of the nanocomposites with 1 and 5 wt % loading are given in Figure 3.

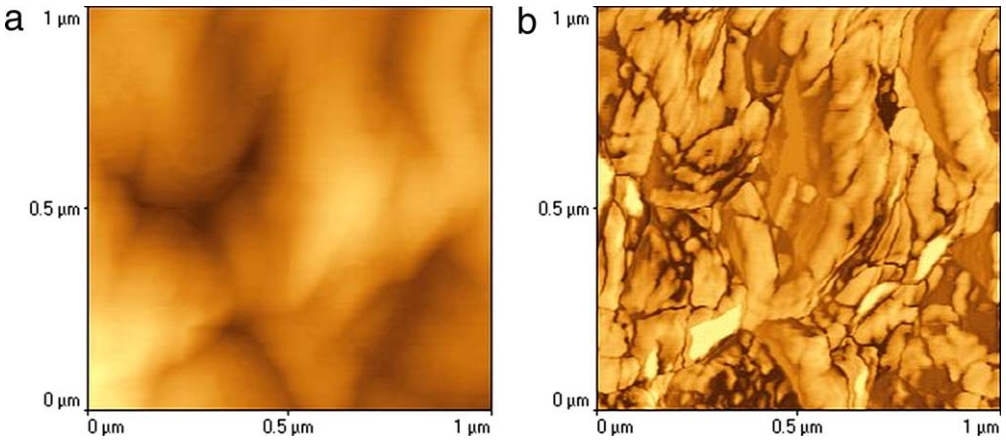

Figure 4. Topography (a) and phase images (b) of pure PHB. [Color figure can be viewed in the online issue, which is available at wileyonlinelibrary.com.]

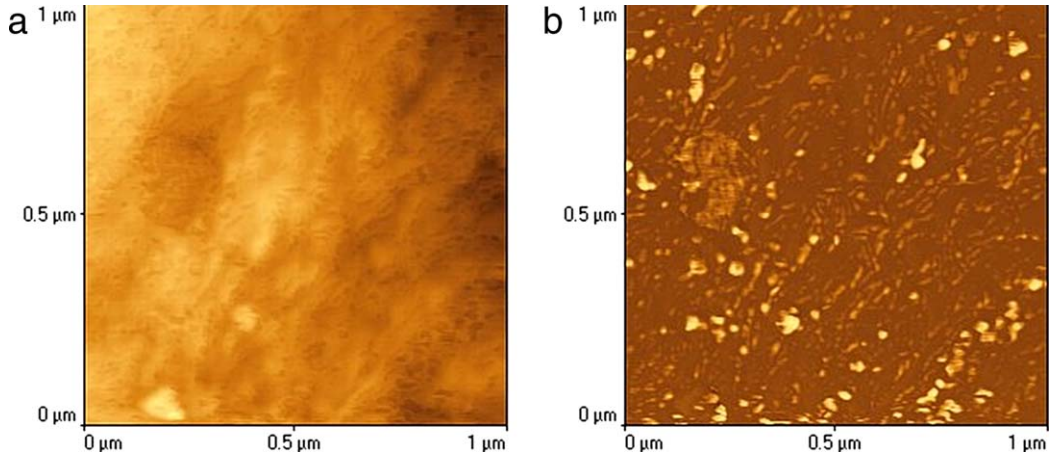

Figure 5. (a) Topography and (b) Phase images of PHB with 5 wt % organically modified MMT (1 × 1 μm). [Color figure can be viewed in the online issue, which is available at wileyonlinelibrary.com.]

The observations of TEM images are consistent with the XRD results in Figure 3. The cross section of the clay layers correspond to the dark lines and the polymer corresponds to the gray area. Figure 3(a) presents the structure of the nanocomposite with 1 wt % C_{18}MMT. The coexistence of both intercalated and exfoliated structures is observed, although the exfoliated structure is the preponderant one. These observations explain the lack of peak in the XRD spectra of the nanocomposite with 1 wt %. The nanocomposite with 5 wt % C_{18}MMT exhibits both structures as well, but the intercalated state is in abundance, as it is shown in Figure 3(b).

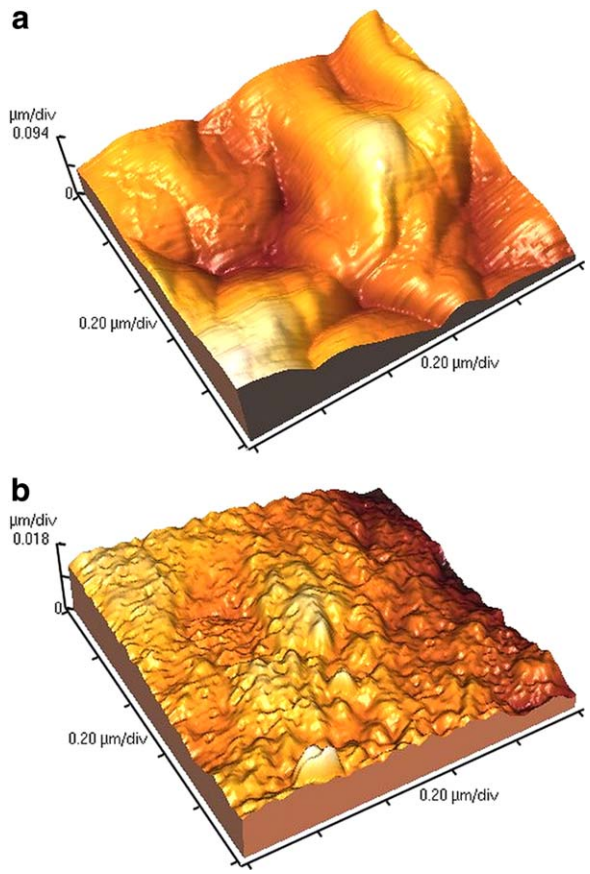

Figure 6. 3D representations of pure PHB (a) and PHB with 5 wt % organically modified MMT (b) (1 × 1 μm). [Color figure can be viewed in the online issue, which is available at wileyonlinelibrary.com.]

This coexistence of the intercalated and the exfoliated states for a wide range of clay loadings was also reported by Marras *et al.*[33]

Atomic Force Microscopy. AFM is a common microscopic method to investigate the surface morphology of polymers[50] and polymer nanocomposites.[33,51] In Figure 4, (a) topography and (b) phase images of pure PHB are shown. Both images correspond to the same sample area. The topography image shows a rather smooth surface, while the phase image revealed a granular structure, which is similar to the structure of polysaccharides.[50]

In Figure 5(a,b), topography and phase images of the nanocomposite PHB with 5 wt % OMMT are shown, respectively. In the phase image, light-colored areas represent the clay aggregates sites (harder material) and the darker areas represent PHB areas. The phase images [Figure 5(b) and similar ones that were taken and are not shown here] reveal a relatively good dispersion of the modified clay inside the PHB matrix.

The 3D representations shown in Figure 6 have been created from the topography images [Figures 4(a) and 5(a)]. The addition of clay increases the surface roughens.

Using the phase image of Figure 7 below, the clay sheets length was measured. This length of 192.36 nm is in good agreement with the length (155.45 nm) of Na montmorillonite's sheets[52] and our TEM observations, as well.

Thermal Behavior

Figure 8 presents the TGA thermographs taken in an inert (N_2) atmosphere at 10°C/min. It is concluded that the thermal degradation mechanism in not affected by the addition of the clay, since the degradation took place in one step for all the samples, as the graphs in Figure 8 show. Since similar results were obtained at different heating rates, the degradation mechanism is not influenced by this factor, the presence of clay.

The TGA curves also show that the addition of the OMMT has improved PHB's thermal behavior. The PHB/C_{18}MMT nanocomposites are more stable compared to pure PHB. The

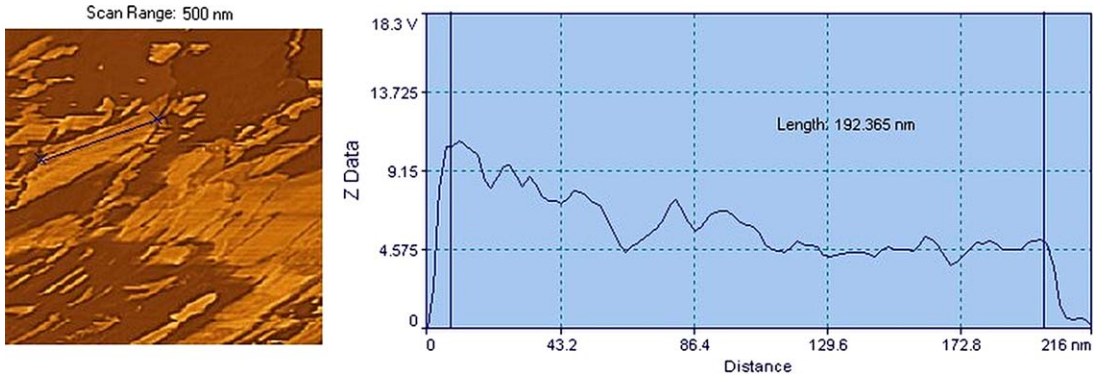

Figure 7. Phase image of PHB with 5 wt % organically modified MMT (500 x 500 nm). Line analysis was performed along the clay sheets. [Color figure can be viewed in the online issue, which is available at wileyonlinelibrary.com.]

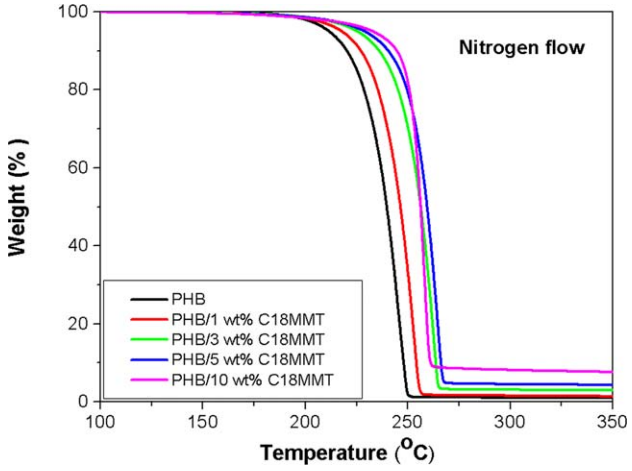

Figure 8. TGA curves of PHB and its nanocomposites with various loadings. [Color figure can be viewed in the online issue, which is available at wileyonlinelibrary.com.]

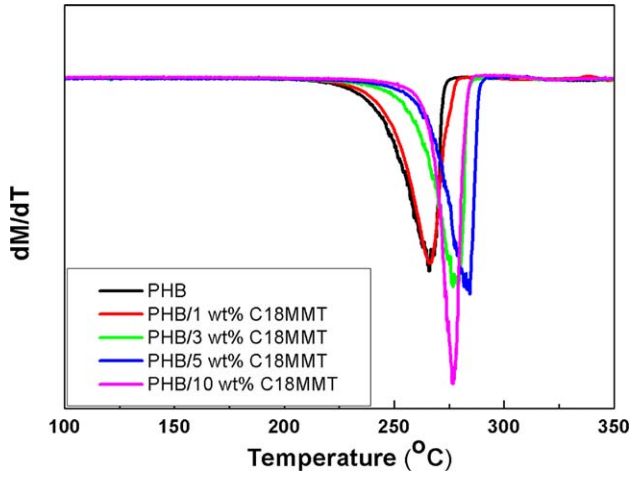

Figure 10. TGA derivative curves of pure PHB and its nanocomposites. [Color figure can be viewed in the online issue, which is available at wileyonlinelibrary.com.]

nanocomposites are more thermally stable as the clay loading increases. The results of Figure 9 show a 26°C rise in the thermal decomposition initiation temperature (at 3% mass loss) between pure PHB and the 10 wt % nanocomposite.

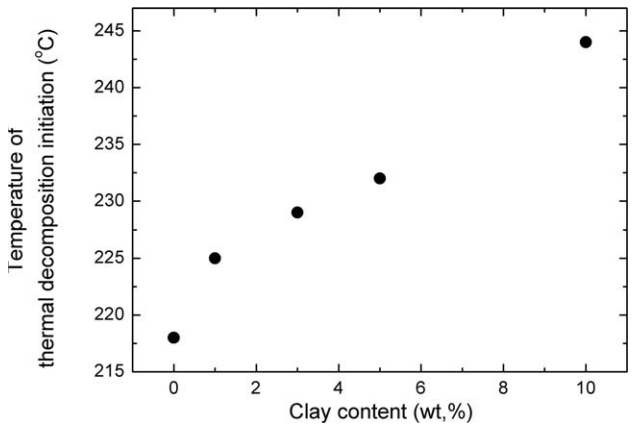

Figure 9. Influence of the organomodified montmorillonite loading on the thermal decomposition initiation temperature.

The thermal stability is enhanced due to the presence of organomodified clay. Similar results have been observed by other researchers.[24,53,54] In Figure 10, TGA derivative thermographs are presented for both the pure polymer and the nanocomposites. It is shown that the peak temperatures are shifted to higher values for the nanocomposites with concentration up to 5 wt %, while for higher concentrations a slightly decrease is observed. Similar results have been observed at various heating rates in a previous work.[55]

DSC was employed to study the melting behavior of all materials. DSC curves are shown in Figure 11. It is significant to note the presence of a second peak in both, the pure PHB and the nanocomposite materials. Possible reasons for the double melting peaks are: (1) melting, subsequent recrystallization, and remelting during heating, (2) polymorphism (different crystal modifications), and (3) different morphology (perfection, distribution and stability of crystals, as well as lamellar thickness).[22,38,56] In order to explain the origin of the two melting endotherms, DSC measurements with different heating rates were performed and are presented in Figure 12. In Figure 12, which corresponds to the nanocomposite with 1% clay loading, two melting peaks are observed. The minor peak corresponds to

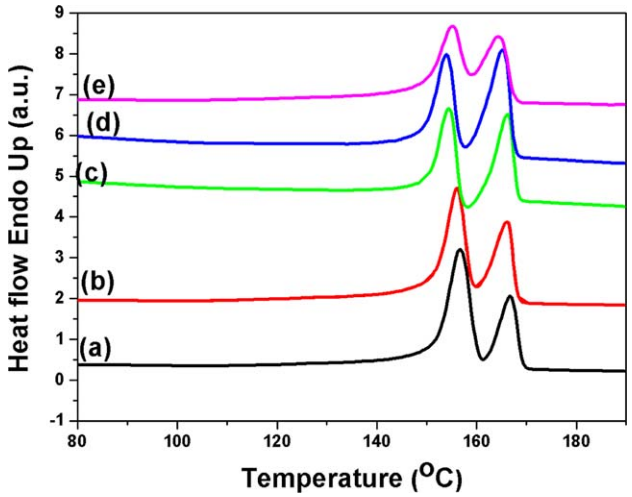

Figure 11. DSC curves of (a) pure PHB and its nanocomposites with (b) 1 wt %; (c) 3 wt %; (d) 5 wt %; and (e) 10 wt % C_{18}MMT. [Color figure can be viewed in the online issue, which is available at wileyonlinelibrary.com.]

the peak, which is observed in the lower temperature, while the major peak corresponds to the peak, which is observed in the higher temperature. It is clearly observed that the intensity of the minor peak is reduced with the increase of the heating rate (from 10 to 20°C/min), while the intensity of the major peak is increased. Moreover, similar results were obtained for the rest of nanocomposites. These observations, in accordance with the literature[57], lead to the conclusion that the minor melting peak should be attributed to recrystallization.

As it is shown in Figure 11, this second peak is not affected by the clay presence, due to the reorganized crystal's melting upon heating.[22]

It is worth noting that, as the clay's loading increases, the first peak is shifted to lower temperatures. That can be explained by the hindrance to the recrystallization phenomenon that the montmorillonite platelets provoke. Less perfect crystals may be induced by the presence of clay platelets and the lower degree

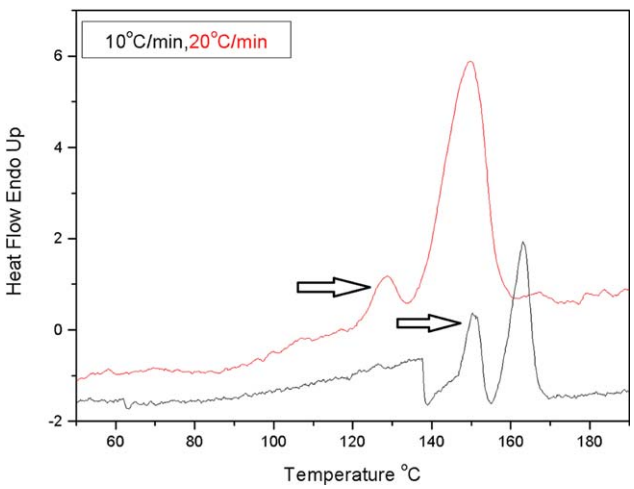

Figure 12. DSC curves for the PHB/1 wt % C_{18}MMT at two different heating rates (10 and 20°C/min). [Color figure can be viewed in the online issue, which is available at wileyonlinelibrary.com.]

Table II. The Thermal, DSC, and TGA, Data for the Neat Polymer and its Nanocomposites with C_{18}MMT

Samples	$T_{m(1)}$[a] (°C)	$T_{m(2)}$[a] (°C)	$T_{on(3\%)}$[b] (°C)	$T_{d(max)}$[c] (°C)	T_{END}[d] (°C)
Pure PHB	156.8	166.8	218	265.7	279.5
PHB/1 wt % C_{18}MMT	156.4	166.13	225	266.6	281.2
PHB/3 wt % C_{18}MMT	154.34	166.13	229	277.5	288.3
PHB/5 wt % C_{18}MMT	153.94	165.53	232	284.2	293.4
PHB/10 wt % C_{18}MMT	154.8	164.53	244	277.1	288.4

[a] $T_{m(1)}$ and $T_{m(2)}$: melting temperatures obtained at the second run.
[b] $T_{on(3\%)}$: the onset decomposition temperature at 3% mass loss.
[c] $T_{d(max)}$: the maximum decomposition rate temperature obtained the DTG peak maximum.
[d] T_{END}: the offset decomposition temperature.

of crystallinity.[22,23] The degree of crystallinity was determined by DSC measurements (not shown here) and it was concluded the addition of clay reduces the PHB crystallinity.

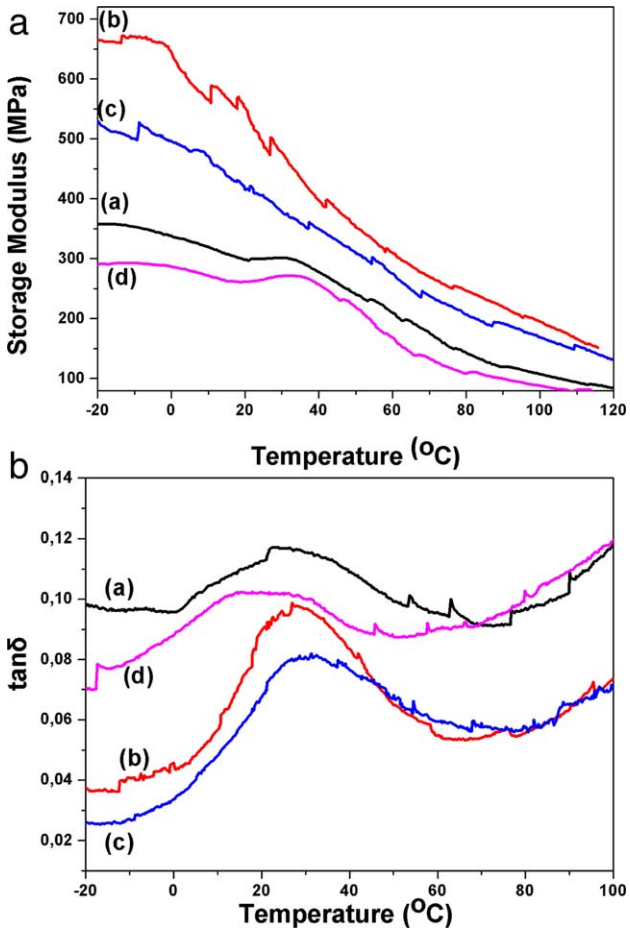

Figure 13. Storage modulus (i) and the loss tangent δ (ii) as a function of temperature of (a) PHB and its C_{18}MMT nanocomposites; (b) 3 wt %; (c) 5 wt %; and (d)10 wt %. [Color figure can be viewed in the online issue, which is available at wileyonlinelibrary.com.]

Table III. DMTA Measurement Results of PHB and its Nanocomposites with Organomontified Montmorillonite

Samples	Storage modulus (20°C) (MPa)	Storage modulus (37°C) (MPa)	T_g (°C) (determined by the peak of the loss tangent δ curve)
Pure PHB	297	287	24.8
PHB/3 wt % C_{18}MMT	552	422	28.2
PHB/5 wt % C_{18}MMT	415	357	29.5
PHB/10 wt % C_{18}MMT	261	267	22.7

Table II shows the overall results relevant to the thermal properties of pure PHB and its nanocomposites.

Dynamic Mechanical Properties

The results from DMTA experiments are presented in Figure 13 and are related to the storage modulus [Figure 13(a)] and the loss tangent δ [Figure 13(b)] of PHB and its nanocomposites. As seen in Figure 13(a), the addition of the clay increases the storage modulus. An increment of 85.6% and of 39.8% is observed for 3 and 5 wt % clay loading at 20°C, respectively. In the current study, the reported increase (45%) in E' is higher than the one in the literature.[24] Moreover in this work, this

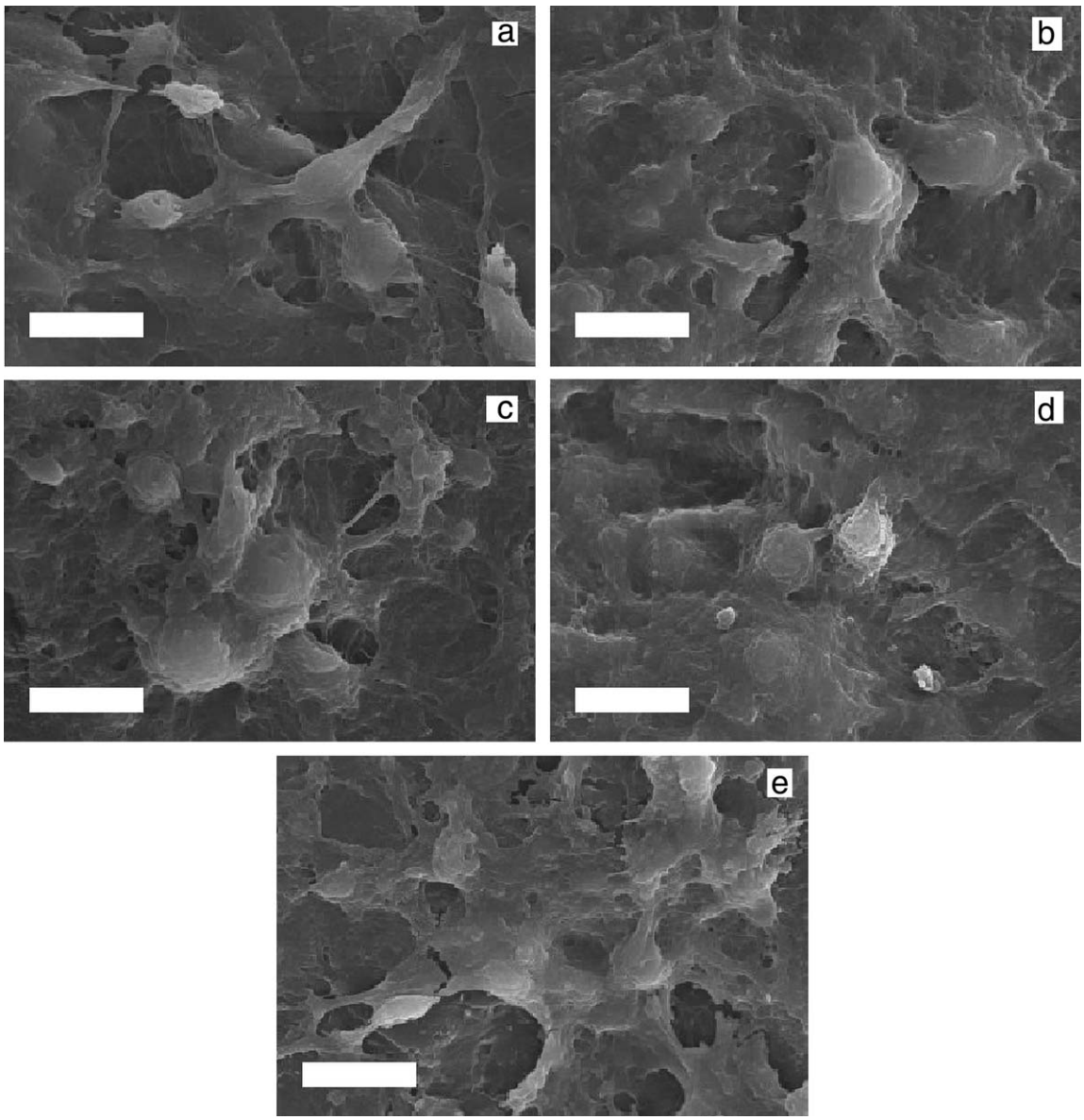

Figure 14. SEM (1400×) imaging of human osteoblasts after 3-day cell culture on (A) pure PHB; (B) PHB/1 wt % clay; (C) PHB/3 wt % clay; (D) PHB/5 wt % clay; (E) PHB/10 wt % clay. The bar is set to 20 μm.

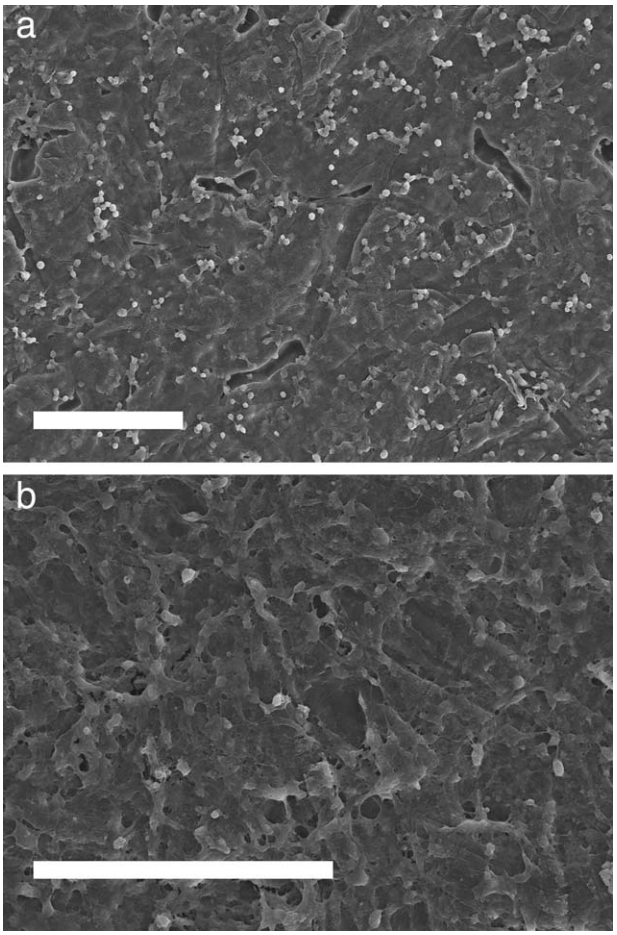

Figure 15. SEM (300×) imaging of human osteoblast cells after 7 days of culture on (a) pure PHB; (b) PHB/5 wt % clay. The bar is set to 200 μm.

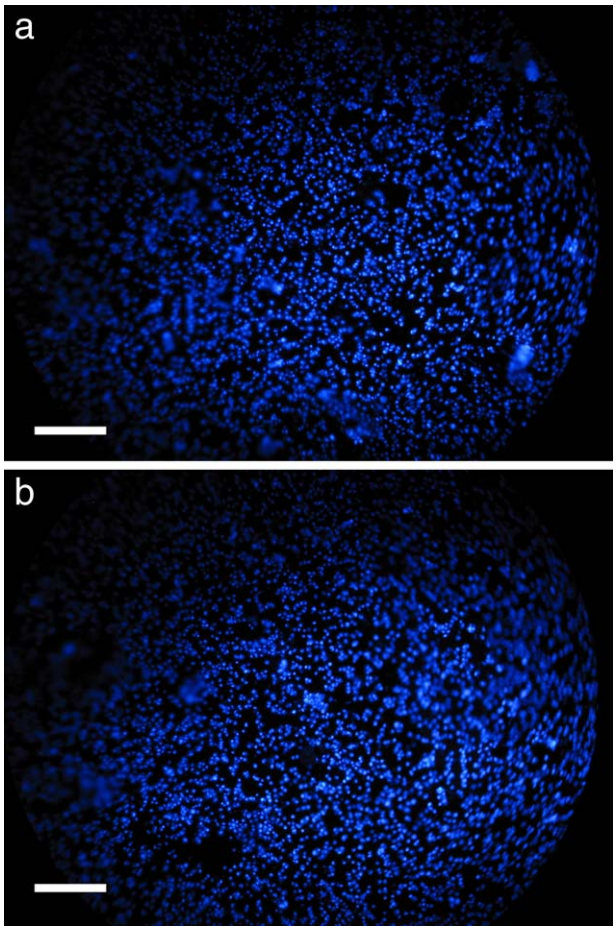

Figure 16. Staining by DAPI of human osteoblast cells after 7 days of culture on (a) pure PHB; (b) PHB/5 wt % clay. The bar is set to 100 μm. [Color figure can be viewed in the online issue, which is available at wileyonlinelibrary.com.]

increase is achieved with lower clay content. As the amount of the nanoclay increases, the increment of the storage modulus decreases. For the nanoclay with 10 wt %, there is a slight decrease, of around 12%, to the storage modulus. These can be attributed to the hydrolysis of the ester bonds of the PHB due to the Al Lewis acid sides, which are present at the edges of the montmorillonite. This provokes a decrease to the molecular weight of the PHB. [21,24] The improvement of mechanical properties can be attributed to the good dispersion of the nanoclays.[23,53] As it is also shown in Figure 13(b), for all the fabricated materials (except for the 10% wt nanocomposite) the glass transition temperature of PHB increases consistently with the addition of the nanofiller. That means that the nanofiller restricts the mobility of the polymeric chains. Similar results have been reported in other studies with hydroxyapatite as the reinforcing nanoparticles.[58]

In Table III, the DMTA results are summarized. The storage modulus at 37°C is also tabulated, since it corresponds to the human physiological temperature. The storage modulus increases approximately 47 and 25% for the 3 and 5 wt % nanocomposites, respectively. A decrease around 7% for the 10 wt % nanocomposite is observed. Similar results, a maximum increment for the storage modulus at a 3 wt % clay loading were reported by Marras *et al.*, who studied the PLLA/clay nanocomposites.[47]

Cell Morphology and Proliferation

In Figure 14, SEM images of cells cultured on pure PHB and PHB/clay nanocomposite substrates (pure, 1, 3, 5, and 10 wt % nanocomposite) are shown. It is observed that, after 3-day culture, the cells are efficiently attached and spread on the PHB/clay nanocomposite surfaces. No significant differences were found among the various substrates. Similar results have been found by Li *et al.*[59] As shown in Figure 15, the physical contact of the spreading cells with each other, through filopodia or lamellipodia, led to large coverage portion of the surface area.

The incorporation of the organo-modified montmorillonite did not affect the adhesion and the spreading of the cells in comparison to those on pure PHB after 3-day culture. Similar proliferation rates were also observed on both substrates in more extended, 7 days, incubation time (Figure 16).

CONCLUSIONS

In this work, nanocomposites of PHB/organo-modified montmorillonite were prepared successfully using the melt-mixing method. The XRD and TEM studies showed that at low clay content (1 wt %) the intercalated and the exfoliated phases coexist, but the exfoliated state dominates. As the clay content

increases, the two states continue to coexist, but the intercalated one prevails. AFM revealed a relatively good dispersion of the OMMT inside PHB in accordance to the TEM imaging. In addition, AFM showed that the nanomposites surface is rougher compared to that of the pristine PHB. PHB's thermal stability was improved with the presence of clay. A critical loading (5 wt %) was found, in which the PHB nanocomposites exhibit maximum thermal stability, 7% greater than that of pure PHB. Moreover, the melting point of the nanohybrids was found to be lower. The addition of the nanoclays improved the thermomechanical properties of the neat polymer. In some cases (3 wt % clay loading, at 20°C), the increase of storage modulus is 85.6%, so the nanocomposite is more rigid than the neat polymer.

The PHB/clay surfaces supported cell attachment and proliferation. This is an indication that the PHB nanocomposites are biocompatible and, therefore, candidate materials for tissue engineering. Further studies, though, are necessary to show whether cell differentiation may be improved on the nanocomposite substrates.

ACKNOWLEDGMENTS

This research has been co-financed by the European Union (European Social Fund, ESF) and Greek national funds through the Operational Program "Education and Lifelong Learning" of the National Strategic Reference Framework (NSRF)—Research Funding Program: Heracleitos II investing in knowledge society through the European Social Fund.

REFERENCES

1. Ikada, Y.; Tsuji, H. *Macromol. Rapid Commun.* **2000**, *21*, 117.
2. Kumar, G. S.; Kalpagam, V.; Nandi, U. S. *J. Macromol. Sci. RMC* **1982**, *22*, 225.
3. Demirbas, A. *Energ. Source Part A* **2007**, *29*, 419.
4. Stein, R. S. *Chem. Eng. News* **2012**, *90*, 2.
5. Lee, S. Y. *Biotechnol. Bioeng.* **1996**, *49*, 1.
6. Gerhart, B.; Klaus, G. L.; Genser, F. *J. Biotechnol.* **1998**, *65*, 127.
7. Reddy, C. S. K.; Ghai, R.; Rashmi Kalia, V. C. *Bioresour. Technol.* **2003**, *87*, 137.
8. Braunegg, G.; Lefebvre, G.; Genser, K. F. *J. Biotechnol.* **1998**, *65*, 127.
9. Keshavarz, T.; Roy, I. *Curr. Opin. Microbiol.* **2010**, *13*, 321.
10. Koller, M.; Salerno, A.; Muhr, A.; Reiterer, A.; Braunegg, G. *Mater. Tehnol.* **2013**, *47*, 5.
11. Muller, H. M.; Seebach, D. *Angew. Chem. Int. Edit.* **1993**, *32*, 477.
12. Barham, P. J.; Keller, A.; Otun, E. L.; Holmes, P. A. *J. Mater. Sci.* **1984**, *19*, 2781.
13. Holmes, P. A. *Phys. Technol.* **1985**, *16*, 32.
14. Zhao, K.; Deng, Y.; Chen, G. Q. *Biochem. Eng. J.* **2003**, *16*, 115.
15. Zhao, K.; Deng, Y.; Chen, J. C.; Chen, G. Q. *Biomaterials* **2003**, *24*, 1041.
16. Chen, G. Q.; Wu, Q. *Biomaterials* **2005**, *26*, 6565.
17. Williams, S. F.; Martin, D. P.; Horowitz, D. M.; Peoples, O. P. *Int. J. Biol. Macromol.* **1999**, *25*, 111.
18. Wu, Q.; Wang, Y.; Chen, G. Q. *Artif. Cell Blood Sub.* **2009**, *37*, 1.
19. Philip, S.; Keshavarz, T.; Roy, I. *J. Chem. Technol. Biotechnol.* **2007**, *82*, 233.
20. Bordes, P.; Hablot, E.; Pollet, E.; Averous, L. *Polym. Degrad. Stab.* **2009**, *94*, 789.
21. Bordes, P. P. E.; Averous, L. *Prog. Polym. Sci.* **2009**, *34*, 125.
22. Bordes, P.; Pollet, E.; Bourbigot, S.; Averous, L. *Macromol. Chem. Phys.* **2008**, *209*, 1473.
23. Botana, A.; Mollo, M.; Eisenberg, P.; Sanchez, R. M. T. *Appl. Clay Sci.* **2010**, *47*, 263.
24. Maiti, P.; Batt, C. A.; Giannelis, E. P. *Biomacromolecules* **2007**, *8*, 3393.
25. Okamoto, M. *J. Ind. Eng. Chem.* **2004**, *10*, 1156.
26. Okamoto, M. Handbook of Biodegradable Polymeric Materials and Their Applications; American Scientific Publishers: Valencia, California, **2005**.
27. Freier, T. *Adv. Polym. Sci.* **2006**, *203*, 1.
28. Rezwan, K.; Chen, Q. Z.; Blaker, J. J.; Boccaccini, A. R. *Biomaterials* **2006**, *27*, 3413.
29. Doyle, C.; Tanner, E. T.; Bonfield, W. *Biomaterials* **1991**, *12*, 841.
30. Shishatskaya, E. I.; Khlusov, I. A.; Volova, T. G. *Biomat. Sci. Polym. E.* **2006**, *17*, 481.
31. Li, H. Y.; Zhai, W. Y.; Chang, J. *J. Biomater. Appl.* **2009**, *24*, 231.
32. Misra, S. K.; Ansari, T. I.; Valappil, S. P.; Mohn, D.; Philip, S. E.; Stark, W. J.; Roy, I.; Knowles, J. C.; Salih, V.; Boccaccini, A. R. *Biomaterials* **2010**, *31*, 2806.
33. Marras, S. I.; Zuburtikudis, I.; Panayiotou, C. *Eur. Polym. J.* **2007**, *43*, 2191.
34. Deligianni, D. D.; Katsala, N. D.; Koutsoukos, P. G.; Missirlis, Y. F. *Biomaterials* **2001**, *22*, 87.
35. Kokkinos, P. A.; Zarkadis, I. K.; Panidis, T. T.; Deligianni, D. D. *J. Mater. Sci. Mater. M.* **2009**, *20*, 655.
36. Sato, H.; Padermshoke, A.; Nakamura, M.; Murakami, R.; Hirose, F.; Senda, K.; Terauchi, H.; Ekgasit, S.; Noda, I.; Ozaki, Y. *Macromol. Symp.* **2005**, *220*, 123.
37. Iwata, T.; Doi, Y. *Macromolecules* **2000**, *33*, 5559.
38. Xie, Y. P.; Noda, I.; Akpaiu, Y. A. *J. Appl. Polym. Sci.* **2008**, *109*, 2259.
39. Xu, J.; Guo, B. H.; Yang, R.; Wu, Q.; Chen, G. Q.; Zhang, Z. M. *Polymer* **2002**, *43*, 6893.
40. Zhang, J. Q.; Kasuya, K.; Hikima, T.; Takata, M.; Takemura, A.; Iwata, T. *Polym. Degrad. Stab.* **2011**, *96*, 2130.
41. Iwata, T. *Macromol. Biosci.* **2005**, *5*, 689.
42. Kabe, T.; Tsuge, T.; Kasuya, K.; Takemura, A.; Hikima, T.; Takata, M.; Iwata, T. *Macromolecules* **2012**, *45*, 1858.
43. Yokouchi, M.; Chatani, Y.; Tadokoro, H.; Teranish, K.; Tani, H. *Polymer* **1973**, *14*, 267.

44. Lauzier, C.; Marchessault, R. H.; Smith, P.; Chanzy, H. *Polymer* **1992**, *33*, 823.
45. Corniber, J.; Marchess, R. H. *J. Mol. Biol.* **1972**, *71*, 735.
46. Pan, P.; Inoue, Y. *Prog. Polym. Sci.* **2009**, *34*, 605.
47. Iwata, T.; Fujita, M.; Aoyagi, Y.; Doi, Y.; Fujisawa, T. *Biomacromolecules* **2005**, *6*, 1803.
48. Aoyagi, Y.; Doi, Y.; Iwata, T. *Polym. Degrad. Stab.* **2003**, *79*, 209.
49. Iwata, T.; Tsunoda, K.; Aoyagi, Y.; Kusaka, S.; Yonezawa, N.; Doi, Y. *Polym. Degrad. Stab.* **2003**, *79*, 217.
50. Karney, G. B.; Butler, P. G.; Scourse, J. D.; Richardson, C. A.; Lau, K. H.; Czernuszka, J. T.; Grovenor, C. R. M. *J. Microsc.* **2011**, *241*, 29.
51. Tsivintzelis, I.; Pavlidou, E.; Panayiotou, C. *J. Supercrit. Fluids* **2007**, *40*, 317.
52. Cadene, A.; Durand-Vidal, S.; Turq, P.; Brendle, J. *J. Colloid Interf. Sci.* **2005**, *285*, 719.
53. D'Amico, D. A.; Manfredi, L. B.; Cyras, V. P. *J. Appl. Polym. Sci.* **2012**, *123*, 200.
54. Bruzaud, S.; Bourmaud, A. *Polym. Test.* **2007**, *26*, 652.
55. Achilias, D. S.; Panayotidou, E.; Zuburtikudis, I. *Thermochim. Acta* **2011**, *514*, 58.
56. Avella, M.; Martuscelli, E.; Pascucci, B.; Raimo, M.; Focher, B.; Marzetti, A. *J. Appl. Polym. Sci.* **1993**, *49*, 2091.
57. Piorkowska, E.; Rutledge, G. C. *Handbook of Polymer Crystallization*; Wiley: Canada, **2013**.
58. Sadat-Shojai, M.; Khorasani, M. T.; Jamshidi, A.; Irani, S. *Mat. Sci. Eng. Mat. Biol. Appl.* **2013**, *33*, 2776.
59. Li, H.; Zhai, W.; Chang, J. *J. Mater. Sci. Mater. M* **2008**, *19*, 67.